Understanding sensitization behavior of lead selenide photoconductive detectors by charge separation model

Lihua Zhao,[a] Jijun Qiu, Binbin Weng, Caleb Chang, Zijian Yuan, and Zhisheng Shi[a]
School of Electrical and Computer Engineering, University of Oklahoma, Norman, Oklahoma 73019, USA

(Received 2 December 2013; accepted 15 February 2014; published online 25 February 2014)

We introduce a charge separation model in this work to explain the mechanism of enhanced photoconductivity of polycrystalline lead salt photoconductors. Our results show that this model could clarify the heuristic fabrication processes of such lead salt detectors that were not well understood and often considered mysterious for nearly a century. The improved lifetime and performance of the device, e.g., responsivity, are attributed to the spatial separation of holes and electrons, hence less possibility of carrier recombination. This model shows that in addition to crystal quality the size of crystallites, the depth of outer conversion layer, and doping concentration could all affect detector performance. The simulation results agree well with experimental results and thus offer a very useful tool for further improvement of lead salt detectors. The model was developed with lead salt family of photoconductors in mind, but may well be applicable to a wider class of semiconducting films. © *2014 AIP Publishing LLC*. [http://dx.doi.org/10.1063/1.4867038]

I. INTRODUCTION

For nearly a century, polycrystalline lead salt film (PbSe and PbS) photoconductive detectors have been widely used for applications in the 1–5 μm spectral range, because of their low cost, ability to operate at room temperature, and high detectivity.[1] However, the operating mechanism of such detectors has not been unambiguously understood. Regardless of deposition techniques, as-grown lead salt polycrystalline films must be thermally treated at certain atmosphere to become sensitive to infrared radiation, being known as sensitization procedure. The detector performance is quite sensitive to many fabrication details such as the size of as-grown crystallites,[2] annealing conditions including atmosphere concentration, temperature, and time,[3–5] number of annealing stages,[3,6] and the final size of crystallites and crystal morphology.[2] Optimization to achieve high performance on such detectors, therefore, becomes an art of trial and error. Understanding the operating mechanism and providing a model that could quantitatively provide guidelines to optimize the experimental conditions are thus very important to further improve such lead salt detectors.

In the past, mainly three theories have been proposed to explain the photoconductivity process.[1,7] The first one accepts the idea that incorporating oxygen in the film sensitizes the infrared photo response, known as the oxidation annealing process.[8–14] This model suggests that oxygen introduces minority carrier traps, which increase the majority carrier lifetime and enhances the photoconductive sensitivity. The second one is based primarily on the increase in the mobility of free carriers in the barrier model. It is assumed that potential barriers are formed during sensitization, either between the crystallites of the film or between n- and p-regions in non-uniform films. The photo-generated electrons and holes could be drawn to and trapped in n- and p-type regions, so that the modulation of barrier could occur under the radiation, to which properties of film, such as photoconductivity and its dependence of temperature and irradiance could be ascribed.[15–19] The third model, referred to as the "generalized theory," was proposed by Petrtiz,[20] in which the properties of film depend on the average properties of many crystallites. The resistivity is related to the boundary barrier, and change in conductivity can be caused by the change in the effective mobility.

Recently, we have pointed out that iodine is the key element in the PbSe photoconductive detector sensitization and demonstrated a record high detectivity.[21] We have also indicated that oxygen serves as an efficient sensitization improver by defect passivation, forming oxide layers at the boundary domain and improving the iodination. Defect passivation by oxygen could be either to eliminate the impurity levels by oxidation of the impurities or to introduce new energy levels that trap the impurity. Either way, the carrier lifetime could be increased. However, lack of details in these previous models made it difficult to optimize lead salt photoconductive detector fabrication. For example, it is not clear how carrier would transport through crystallites boundaries. Since iodine is an n-type dopant for PbSe, our study led us to believe that the p-n junction model is the case. The built-in potential of the p-n junction spatially separates photon-induced electrons and holes at a rate faster than Auger and radiative recombination, which suppressed PL emission. This also agrees well with our experiment that there was no observable photoluminescence for samples with high responsivity after iodination. In this work, we present a charge separation model that allows us to do some quantitative simulations to explain the experimental results and provide some guidelines for fabrication. As an example simulation, p-type PbSe is used. The surfaces of p-type polycrystalline PbSe were converted into n-type to form p-n junctions during the sensitization process.[22,23] In addition, it is also

[a]Authors to whom correspondence should be addressed. Electronic addresses: lihua.zhao@ou.edu and shi@ou.edu.

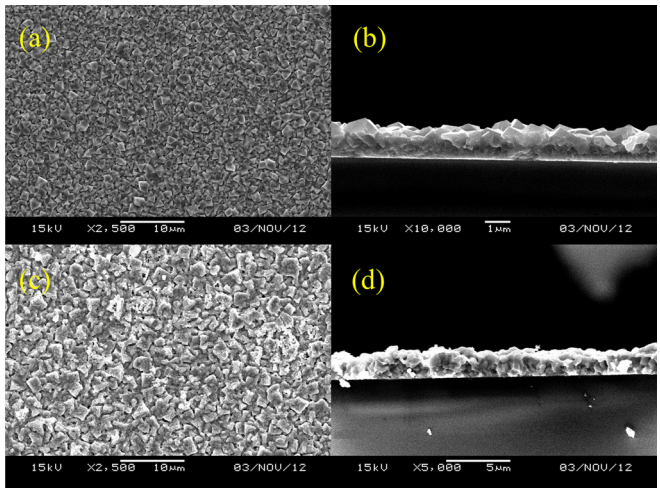

FIG. 1. Scanning electron microscope (SEM) pictures of polycrystalline PbSe structure before (a) and (b), and after (c) and (d) sensitization.

considered that electrons and holes will transport in n- and p-type channels, respectively. Under these conditions, detectors could benefit from enhanced carrier lifetime to achieve high performance. The model was developed with lead salt family of photoconductors in mind, but may well be applicable to a wider class of semiconducting films. In our previous experiments, the p-type polycrystalline PbSe films were fabricated by using chemical bath deposition and then sensitized. The sensitization consists of two steps, which are annealing in air as the pretreatment followed by annealing in iodine atmosphere. Fig. 1 shows scanning electron microscope pictures of polycrystalline PbSe structure before and after sensitization. One could see that during the sensitization, the as-grown polycrystalline PbSe would recrystallize to form crystallites with sizes from 100 nm to 500 nm. Under certain sensitization conditions majority of crystallites will have a similar size.

II. SIMULATION MODEL

In the previous p-n junction/barrier models, all surfaces of crystallites are surrounded by p-n junctions and/or oxide barrier layers.[10,20] Therefore, carriers will have to tunnel through many junctions/oxide barriers. There are two problems with those models. One is that the resistance estimated is much larger than the experimental value. Another is that fast carrier recombination will occur when majority carriers travelling through barriers into other conductive type area (hole into n-area, or electrons into p-area), which would reduce carrier lifetime and responsivity significantly. To solve those discrepancies in the previous model, we propose in this paper that during the high temperature sensitization process crystallites will randomly make interconnections to form threading micro-crystallites and thus create conducting channels for the carriers in the crystallite core to transport through. In such threading micro-crystallites, holes in the crystallite core will transport through the conducting channels (threads), while electrons will transport through interconnected outer surfaces. Therefore, carrier recombination will be significantly reduced with electrons and holes traveling in their own lanes. Although the interconnections could be random in all directions, under bias the carrier could statistically transfer through this channel along the bias direction. Fig. 2 depicts our model. In Fig. 2(a), the dark color presents p-type region and light color represents n-type region with a diffusion doping profile into the crystallite core. The n-type outer shell could include oxide layers such as PbO or a mixture of PbO_xSe_{1-x} and halogens.[23] The blue solid and red dashed lines represent example of electron-channel in outer shell and hole-channel in core p-type PbSe crystallites, respectively. Fig. 2(b) shows two-layer crystallites represented by connected spheres. Fig. 2(c) shows a single crystallite in our model for carrier concentration calculation.

Hall measurements show that polycrystalline PbSe films without iodine are p-type with hole concentration around $1 \times 10^{17}\,cm^{-3}$. Thus, the initial acceptor concentration (N_A) in p-type PbSe crystallites before introducing n-type inversion layer is taken as $1 \times 10^{17}\,cm^{-3}$. For n-type inversion region, average donor concentration (N_D) is initially assumed to be $1 \times 10^{17}\,cm^{-3}$. Different N_D will be discussed later. In addition, N-type diffusion profile was neglected in the simulation. Electron concentration in the outer shell and hole concentration in the core were thus simulated.[24] Fig. 3 shows electrons and holes concentration distribution for D = 500 nm and dn = 10 nm, the black dashed line indicates

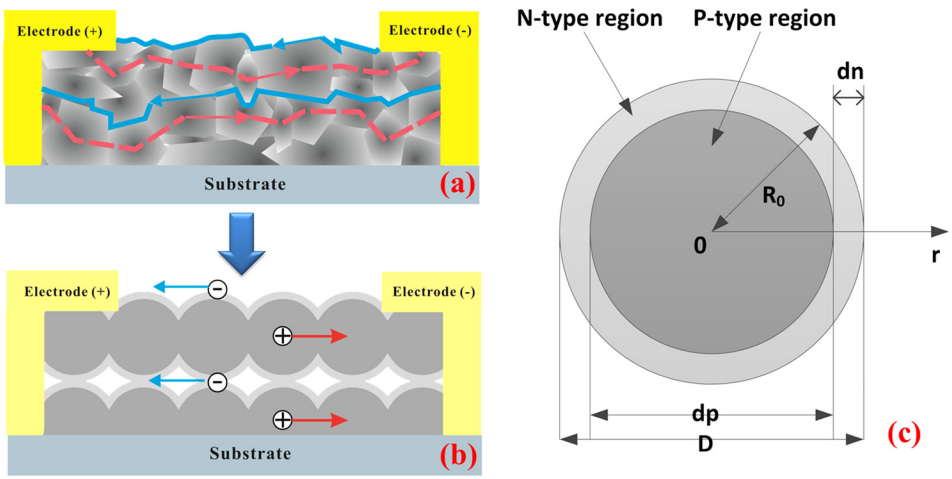

FIG. 2. (a) Our proposed model that shows the surfaces of crystallites are converted from p-type into n-type. (b) Polycrystalline PbSe represented by spheres used in the model, in which one sphere represents one single crystallite. (c) Structure used in carrier concentration simulation, where p-type region is surrounded by n-type region. D presents diameter of sphere, R_0 is the radius of sphere, dp is size of p-type region, and dn is depth of n-type region, D = dp + 2*dn.

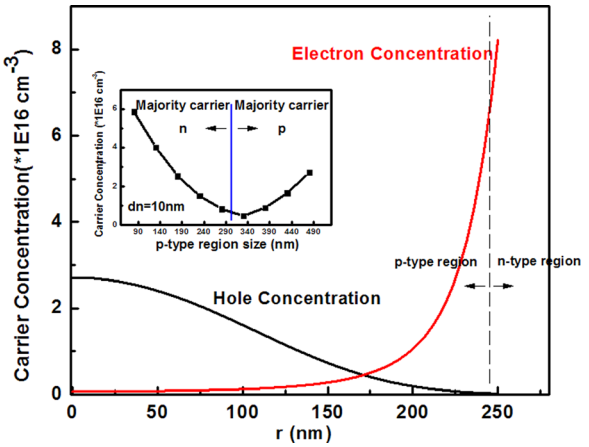

FIG. 3. Carrier concentration distribution inside the sphere, red line: electron, black line: hole. Inset: Size dependent majority carrier concentration at sphere center.

the position of n- and p-type region boundary. The relation of majority carrier concentrations at sphere center and sphere size is also shown as the inset, in which dn = 10 nm. When p-type region size is less than 300 nm, majority carrier at center of sphere becomes n-type, which suggest over iodization could cause type conversion. Our experiments indicate that over iodization especially on small size crystallites always led to poor optical response. In the following simulations, we will focus on cases that p-n junctions exit.

As can be seen, with proper sensitization p-n junction will be formed and the hole carrier concentration is significantly reduced due to such charged region. Therefore, a reduced carrier recombination and enhanced lifetime are expected. This could be understood by the following equation:

$$R_{total} = r_{rad}np + r_{Aug-e}n^2p + r_{Aug-h}np^2 + \frac{N_{rec}}{\tau_{SRH-e}} + \frac{P_{rec}}{\tau_{SRH-p}}. \quad (1)$$

In the equation, R_{total} is total recombination rate, r_{rad} is radiative recombination coefficient, n is electrons concentration, p is holes concentration, $r_{Aug\text{-}e}$ is Auger electrons recombination coefficient, $r_{Aug\text{-}h}$ is Auger holes recombination coefficient, $\tau_{SRH\text{-}e}$ is electrons lifetime of Shockley-Read-Hall (SRH) recombination, $\tau_{SRH\text{-}h}$ is holes lifetime of Shockley-Read-Hall recombination, N_{rec} and P_{rec} are recombination center concentration for electrons and holes, respectively. Based on our previous studies,[21,25] we assume that defects are well passivated during the sensitization process and, therefore, radiative and Auger lifetimes are dominant.

Radiative and Auger lifetime could be calculated from Refs. 26–28. Fig. 4(a) shows the lifetime in PbSe based on our model for different sizes. One could see that the lifetime is increased to as long as 0.31 μs, which is almost 40 times larger than that of 7 ns before sensitization.

III. SIMULATION RESULTS AND DISCUSSION

With the lifetime, the photo responsivity could be estimated as $Rs = q\eta\tau\mu\lambda V/hcl^2$,[29] where η is efficiency, τ is carrier lifetime, V is applied voltage, μ is the carrier mobility, λ is the wavelength of incident power, h is Planck's constant, c is light velocity, and l is the dimension of detector. The ratio between the responsivity of after ($R_{sensitized}$) and before (R_{before}) sensitization is shown in Fig. 4(b). Responsivity could be enhanced by approximately as large as 45 times. This simulation could help explain why we did not observe good photon response from PbSe materials without iodine and very high response after iodine sensitization that we believe has introduced p-n junctions. Fig. 4 also indicates that the device performance is very sensitive to the final crystallites size, which depends on as-grown crystallites size and annealing conditions. The doping concentration also affects the performance, which also depends on sensitization conditions.

This simulation could also help explain another key unexplained mystery that manipulating the resistance during

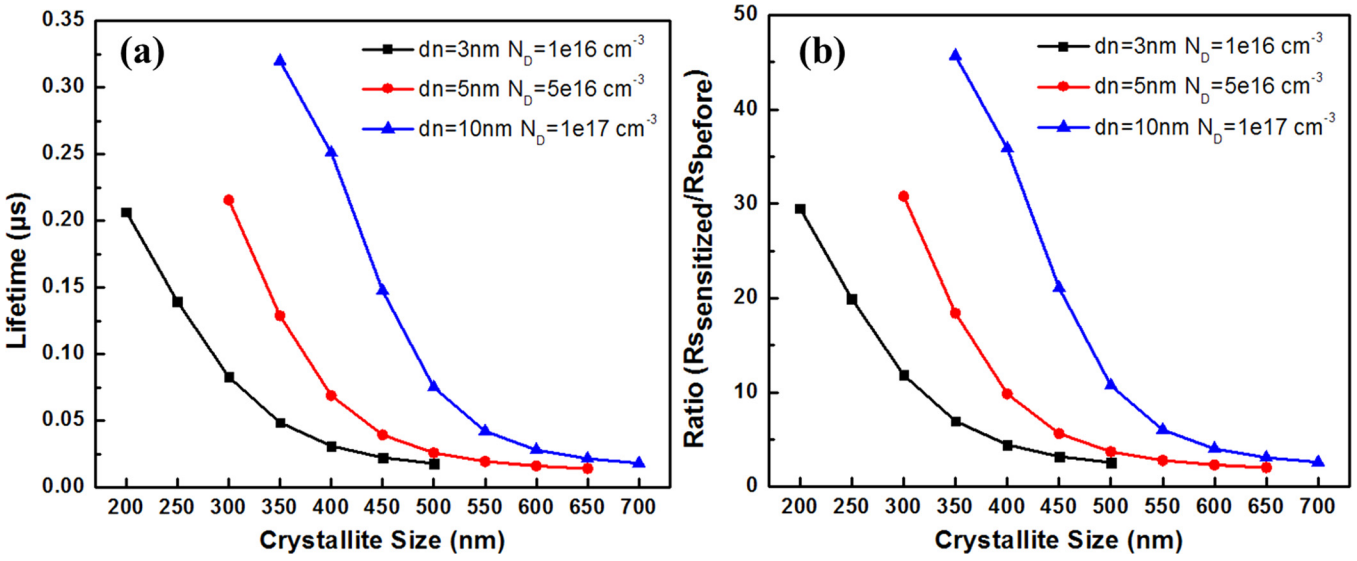

FIG. 4. (a) Simulated lifetime in PbSe. (b) A ratio between the responsivity of after ($Rs_{sensitized}$) and before (Rs_{before}) sensitization versus different crystallites sizes. dn = 3 nm ($N_D = 1 \times 10^{16}$ cm^{-3}), 5 nm ($N_D = 5 \times 10^{16}$ cm^{-3}), and 10 nm ($N_D = 1 \times 10^{17}$ cm^{-3}).

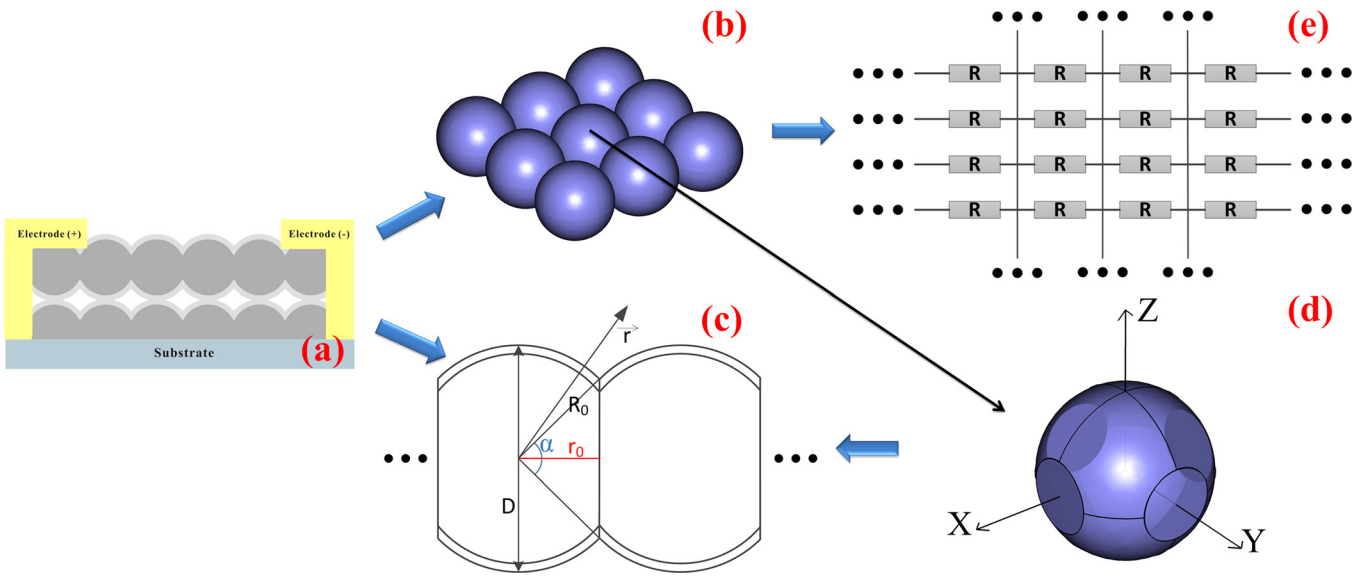

FIG. 5. Model for resistance simulation.

sensitization process is a critical factor to achieve high sensitivity in PbSe photoconductive detector fabrication. Since the resistance of the PbSe films depends on the size of the crystallites and carrier concentration after sensitization which in turn determines the responsivity, it is, therefore, understandable that resistance could be used to optimize detector performance. In the following simulations, we will calculate resistance and provide guideline to explain it.

Fig. 5 shows our model for resistance calculation. The basic resistance unit in sphere matrix is shown in Fig. 5(d). The resistance of integral sphere will be calculated first, and then resistance in the overlap part as is shown in Fig. 5(c) will be subtracted since they connect in series. From Fig. 5(c), one could see 2-dimension relationship of two adjacent spheres. The resistance of integral sphere R_{sp} could be calculated by the following equation:

$$R_{sp} = \int_{\delta r}^{R_0} \frac{\rho}{4\pi r^2} dr, \tag{2}$$

where ρ is the resistivity, R_0 is the radius of the sphere and $R_0 = D/2$. To avoid singularity, the lower limit of integration is set to be an infinitesimal δr, which means the resistance at center of sphere is neglected. ρ follows the equation $\rho = 1/\sigma = 1/(q^*\mu_n{}^*n(r) + q^*\mu_p{}^*p(r))$, where q is the electron charge, μ_n and μ_p are mobility of electrons and holes at room temperature, respectively. n(r) and p(r) are calculated numerically as shown in Fig. 3 The resistance for the overlap part R_{so} could be calculated by

$$R_{so} = \int_{r_0+\delta r}^{R_0} 2\pi\rho\left(1 - \frac{r_0}{r}\right) r^2 dr, \tag{3}$$

where r_0 is distance from sphere center to the cross section of overlap part as shown in Fig. 5(c). Finally, the resistance for one unit in the sphere matrix is $R_u = R_{sp} - 4^*R_{so}$.

To simplify the calculation, we consider one unit resistor shown in Fig. 5(b), and all resistors are connected to form a resistor matrix as shown in Fig. 5(e). According to the Kirchhoff law, the overall resistance for resistor matrix Rt could be expressed by the following equation:

$$Rt = \frac{2}{\pi}\sum_{m=1}^{N} \frac{R_u}{2m-1}, \tag{4}$$

where N is the number of spheres in one layer of film and could be estimated from the dimension of film and diameter of sphere. The final resistance for the PbSe film (R) is parallel resistance of layers. Fig. 6 shows calculated results of film resistance versus different crystallite sizes and dn.

To compare with our experimental results, the dimension of the film in the simulation is chosen as 1 mm × 1mm and 1 μm thick. Herein, r_0 is taken as $r_0 = R_0{}^*\cos(\pi/12)$, which means the α in Fig. 5(c) is $\pi/6$. The simulated resistance value ranges from 1 MΩ to 18 MΩ. Our calculated

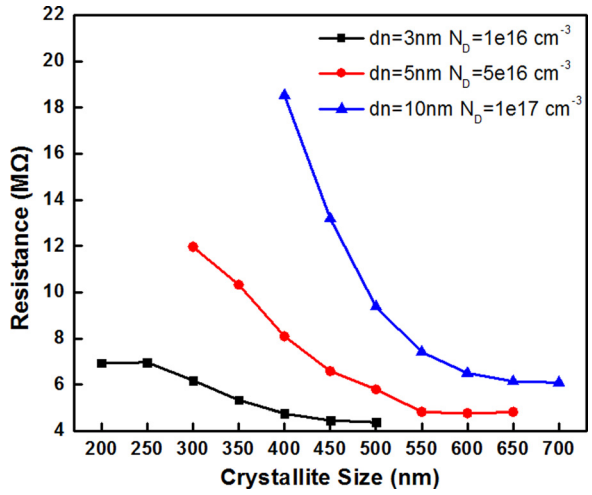

FIG. 6. Film resistance (R) versus different crystallites sizes (D) with different n-type regions. dn = 3 nm ($N_D = 1 \times 10^{16}$ cm^{-3}), 5 nm ($N_D = 5 \times 10^{16}$ cm^{-3}), and 10 nm ($N_D = 1 \times 10^{17}$ cm^{-3}).

resistance values are somewhat larger than our experimental results (0.5 MΩ to 10 MΩ). This could be attributed to (1) that the number of conducting channels used in our model is less than reality, (2) hypothesis of no cross talk between crystallites layers, (3) two dimensional model instead of three dimensional model. Nonetheless, this model offers following hints for a good sensitization. (1) Low resistance would suggest high concentration in crystallites and thus high recombination. (2) There is a resistance range that indicates p-n junction formation. (3) When resistance becomes too high, it may suggest that most of the conducting channels are closed by oxides. This could explain why good detectors always fall into a certain resistance range. As can be seen from our model, the optimized resistance value depends on the size of crystallites and the sensitization condition. With different doping concentration used in our simulation, the best devices could come from films with crystallites size approximately from 250 nm to 450 nm, in which highest carrier lifetime is obtained due to charge separation. In this work, we did not consider the influence of sensitization on the carrier mobility, which could be our future work.

IV. CONCLUSIONS

In summary, we have presented a charge separation model to explain the mechanism of polycrystalline lead salt photoconductors. The improved lifetime and performance of the device, e.g., responsivity, are attributed to the spatial separation of holes and electrons which reduces carrier recombination. These results provide guidelines for further detector optimization. We believe this model could also be used for other semiconductors and other type of devices as well.

ACKNOWLEDGMENTS

The authors acknowledge funding support for this work provided by the DoD AFOSR under Grant No. FA9550-12-1-0451, DoD ARO Grant No. W911NF-07-1-0587, and by Oklahoma OCAST program under Grant Nos. AR112-18 and AR132-003.

[1]A. Rogalski, *Infrared Detectors*, 2nd ed. (Taylor and Francis Group, LLC and CRC Press, 2011).
[2]A. Munoz, J. Melendez, M. C. Torquemada, M. T. Rodrigo, J. Cebrian, A. J. de Castro, J. Meneses, M. Ugarte, F. Lopez, G. Vergara, J. L. Hernandez, J. M. Martın, L. Adell, and M. T. Montojo, Thin Solid Films **317**, 425 (1998).
[3]J. N. Humphrey and R. L. Petritz, Phys. Rev. **105**, 1736 (1957).
[4]Y. Yasuoka and M. Wada, Jpn. J. Appl. Phys., Part 1 **13**, 1797 (1974).
[5]F. Briones, D. Golmayo, and C. Ortiz, Thin Solid Films **78**, 385 (1981).
[6]R. M. Candea, R. Turcu, G. Borodi, and I. Bratu, Phys. Status Solidi A **100**, 149 (1987).
[7]D. E. Bode, "Lead salt detectors," in *Physics of Thin Films*, edited by G. Hass and R. E. Thun (Academic Press, New York, 1966), pp. 275–301, Vol. 3.
[8]D. E. Bode and H. Levinstein, Phys. Rev. **96**, 259 (1954).
[9]R. H. Harada and H. T. Minden, Phys. Rev. **102**, 1258 (1956).
[10]J. N. Humphrey and W. W. Scanlon, Phys. Rev. **105**, 469 (1957).
[11]T. H. Johnson, Proc. SPIE **0443**, 60 (1983).
[12]S. Gorer, A. Albu-Yaron, and G. Hodes, Chem. Mater. **7**, 1243 (1995).
[13]J. Wang, J. Hu, P. Becla, A. M. Agarwal, and L. C. Kimerling, J. Appl. Phys. **110**, 083719 (2011).
[14]V. T. Trofimov, G. Yu, and E. G. Chizhevskii, Fiz. Tekh. Poluprovodn. (S.-Peterburg) **30**, 755 (1996).
[15]E. S. Rittner, Science **111**, 685 (1950).
[16]A. F. Gibson, Proc. Phys. Soc. B (London) **64**, 603 (1951).
[17]H. T. Minden, J. Chem. Phys. **23**, 1948 (1955).
[18]J. C. Slater, Phys. Rev. **103**, 1631 (1956).
[19]S. Horn, D. Lohrmann, P. Norton, K. McCormack, and A. Hutchinson, Proc. SPIE **5783**, 401 (2005).
[20]R. L. Petritz, Phys. Rev. **104**, 1508 (1956).
[21]J. Qiu, B. Weng, Z. Yuan, and Z. Shi, J. Appl. Phys. **113**, 103102 (2013).
[22]S. Espevik, C. Wu, and R. H. Bube, J. Appl. Phys. **42**, 3513 (1971).
[23]M. C. Torquemada, M. T. Rodrigo, G. Vergara, F. J. Sánchez, R. Almazán, M. Verdú, P. Rodríguez, V. Villamayor, L. J. Gómez, and M. T. Montojo, J. Appl. Phys. **93**, 1778 (2003).
[24]S. M. Zse, *Physics of Semiconductor Devices*, 2nd ed. (John Wiley & Sons, 1981).
[25]F. Zhao, J. Ma, D. Li, S. Mukherjee, G. Bi, and Z. Shi, J. Electron. Mater. **38**, 1661 (2009).
[26]O. Ziep, D. Genzow, M. Mocker, and K. H. Herrmann, Phys. Status Solidi B **99**, 129 (1980).
[27]A. Rogalski and W. Larkowski, Electron Technol. **18**, 55 (1985).
[28]P. R. Emtage, J. Appl. Phys. **47**, 2565 (1976).
[29]E. Rosh and B. Vinter, *Optoelectronics* (Cambridge University Press, 2004).